

# Estimating Lyapunov exponents in billiards

George Datsleris,<sup>\*</sup> Lukas Hupe,<sup>†</sup> and Ragnar Fleischmann  
*Max Planck Institute for Dynamics and Self-Organization and  
Faculty of Physics, Georg-August-Universität Göttingen*  
(Dated: April 8, 2022)

Dynamical billiards are paradigmatic examples of chaotic Hamiltonian dynamical systems with widespread applications in physics. We study how well their Lyapunov exponent, characterizing the chaotic dynamics, and its dependence on external parameters can be estimated from phase space volume arguments, with emphasis on billiards with mixed regular and chaotic phase spaces. We show that the leading contribution to the Lyapunov exponent is generically inversely proportional to the chaotic phase space volume. We also present a numerical scheme and software implementation to calculate the Lyapunov exponents for billiards in external magnetic fields.

## I. INTRODUCTION

Dynamical billiards are a well-studied class of dynamical systems, having applications in many different fields of physics. Besides playing a prominent role in ergodic theory [1–3], billiards are important example systems for understanding quantum chaos [4, 5], with practical applications e.g. in modelling optical microresonators for lasers [6, 7] and room acoustics [8]. Billiard-models have also been particularly successful in helping to understand transport properties of electronic nanostructures such as quantum dots and antidot super-lattices [9–18].

A billiard consists of a finite (or periodic) domain in which a point particle performs free flight with unit velocity. Upon collision with the boundary of the domain the particle (typically) is specularly reflected. In Fig. 1 we are showing the two example billiards we will be considering in this paper: the mushroom billiard (MB) and the periodic Sinai billiard without (PSB) and with magnetic field (MPSB).

An essential characterization of the chaotic dynamics of a billiard is of course provided by its Lyapunov exponents. For a two dimensional billiard the Lyapunov exponents are four numbers  $\lambda_{1-4}$  that measure how “chaotic” the billiard is, in terms of the average exponential rates of expansion (and contraction) of the phase space along certain characteristic directions. Due to the Hamiltonian nature of the dynamics, the Lyapunov exponents fulfil  $\lambda_1 = -\lambda_4, \lambda_2 = \lambda_3 = 0$ . Therefore in the remainder of the text we will be only considering the largest exponent  $\lambda \equiv \lambda_1$ . The fundamental mathematical properties of the Lyapunov exponents in billiards, including rigorous proofs of their existence, have been studied in literature and can e.g. be found in Ref. [19–21] and references therein.

Quantitative studies of the Lyapunov exponent in actual physical billiards are surprisingly rare however. A computational framework for calculating  $\lambda$  in billiard systems was formulated by Dellago, Posch, and Hoover in

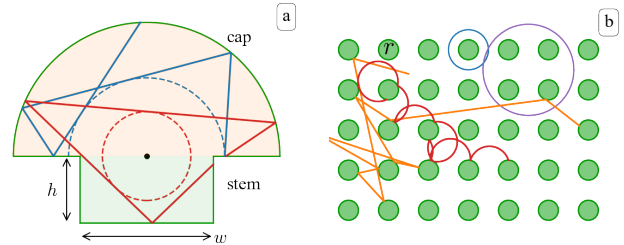


FIG. 1. (a) A regular (blue) and chaotic (red) orbit in the mushroom billiard (MB), whose cap radius is a constant set to 1. The cap and the stem are separated with different background colors (orange, green). (b) chaotic orbits without (orange) and with (red) magnetic field and regular orbits (blue, purple) in the magnetic periodic Sinai billiard (MPSB).

Refs. [22, 23] (to which we refer to as *DPH framework* in the following, and which we will extend to the dynamics in magnetic fields). In literature, Lyapunov exponents have been computed for the PSB on square [24] and hexagonal [22, 24] lattices, as well as for the stadium billiard [22, 25], which is related to the mushroom billiard. Furthermore, there are results for the magnetic elliptical billiard [26] and the inverse magnetic stadium [27].

All these quantitative calculations rely on detailed numerical simulations of the complex billiard dynamics. In this paper, however, we want to follow a different approach exploring approximate expressions for the parameter dependence of the Lyapunov exponents in some paradigmatic cases, especially of billiards with *mixed* phase space, where regions of regular and chaotic dynamics coexist. Our work is motivated by a recent study that has shown that magnetoresistance measurements in graphene and semiconductor nanostructures directly reflect the parameter dependence of the chaotic phase space volume [9]. This is due to the fact, that characteristic transport times in the chaotic sea are fundamentally linked to the respective volume fraction of the chaotic phase space in the corresponding billiards. Namely, for the magnetic periodic Sinai billiard (MPSB) in Fig. 1b it

<sup>\*</sup> george.datsleris@ds.mpg.de

<sup>†</sup> GD and LH contributed equally to this work

was analytically shown that the mean collision time  $\kappa(B)$  between successive collisions with the discs (of radius  $r$ ) as a function of an applied external magnetic field  $B$  is equal to the varying chaotic phase space portion  $g_c(B)$  times the value of  $\kappa(0)$  at zero magnetic field, i.e.

$$\kappa(B) = g_c(B) \times \kappa(0) = g_c(B) \times \frac{1 - \pi r^2}{2r}. \quad (1)$$

(The value of  $\kappa(0)$  is obtained from Eq. (3) below.)

The Lyapunov exponents in billiards are also linked to the mean collision times as the following back-of-the-envelope calculation motivates. Let us study the perturbation growth, i.e. the exponential growth of the phase space distance  $|\delta\mathbf{\Gamma}(t)|$  of two initially infinitesimally close by trajectories. The origin of the exponential perturbation growth and thus of chaos in billiards are collisions with curved boundaries [28]. Assuming an average perturbation growth increase of  $C$  between collisions with curved boundaries and an average time  $\langle\Delta t\rangle = \kappa$  between such collisions, one would expect a perturbation growth of  $|\delta\mathbf{\Gamma}(t)| \approx C^{t/\kappa} |\delta\mathbf{\Gamma}(0)|$ . This means for the Lyapunov exponent (see definition in Eq. (4) below) we expect

$$\lambda \approx \frac{\log(C)}{\kappa}. \quad (2)$$

In general billiards have non-curved boundaries as well as curved ones, thus  $\kappa \neq \tau$ . Here  $\tau$  is the mean collision time with the boundary of the billiard that is known analytically for *any* billiard and is given by

$$\tau = \frac{\pi|Q|}{|\partial Q|} \quad (3)$$

where  $|Q|$  is the area of the billiard and  $|\partial Q|$  the total length of its boundary [19].

The aim of this paper is to explore how far phase space volume considerations like Eq. (1) allow us to estimate the parameter dependence of the Lyapunov exponent in billiard systems. To this end we will analyze the contributions to the approximate expression (2) and compare it with detailed numerical simulations. In sec. II we provide the basic framework we will use for computing  $\lambda$ , as well as apply the aforementioned back-of-the-envelope calculation to realistic perturbation growth. Following in sec. III we present our results and then conclude by pointing out the generality of our approach.

## II. LYAPUNOV EXPONENTS IN BILLIARDS

In this section we first give a brief overview of the DPH framework [22, 23] for numerically computing  $\lambda$ , reciting the equations that will be relevant for our study. We will then extend the framework to motion in an external magnetic field. (In the following we will assume that the point particle in the billiard has unit mass and momentum and velocity are the same.)

The (maximum) Lyapunov exponent is defined based on the evolution of the four-dimensional perturbation vector  $\delta\mathbf{\Gamma} = (\delta\mathbf{q}, \delta\mathbf{p})^T$  as

$$\lambda_{\mathbf{\Gamma}(0), \delta\mathbf{\Gamma}(0)} = \lim_{t \rightarrow \infty} \frac{1}{t} \log \frac{|\delta\mathbf{\Gamma}(t)|}{|\delta\mathbf{\Gamma}(0)|} \quad (4)$$

with  $\delta\mathbf{\Gamma}$  evolving according to the evolution equations in tangent space,  $\delta\mathbf{\Gamma} = J(\mathbf{\Gamma}(t)) \cdot \delta\mathbf{\Gamma}$  where  $J$  is the Jacobian matrix of the equations of motion. For all  $\mathbf{\Gamma}(0)$  inside an ergodic component of phase space the value of  $\lambda$  does not depend on the initial condition.

### A. Without magnetic field

The time evolution in tangent space for a particle moving in a straight line is

$$\delta\mathbf{\Gamma}(t) = \begin{pmatrix} \mathbb{I}_{2 \times 2} & t \cdot \mathbb{I}_{2 \times 2} \\ 0_{2 \times 2} & \mathbb{I}_{2 \times 2} \end{pmatrix} \delta\mathbf{\Gamma}(0). \quad (5)$$

At discrete time points Eq. (5) is interrupted by collisions with the boundary and the perturbation vector changes discontinuously. The perturbation vector just after the collision (we'll use  $'$  to label quantities right after the collision) is derived from the one just before the collision as [23]

$$\delta\mathbf{\Gamma}' = \begin{pmatrix} \delta\mathbf{q} - 2(\delta\mathbf{q} \cdot \mathbf{n}) \mathbf{n} \\ \delta\mathbf{p} - 2(\delta\mathbf{p} \cdot \mathbf{n}) \mathbf{n} - 2\gamma_r \frac{(\delta\mathbf{q} \cdot \mathbf{e})}{\cos\phi} \mathbf{e}' \end{pmatrix} \quad (6)$$

for a collision with a boundary segment of curvature  $\gamma_r$ . The two types of boundaries we will encounter in this work are straight walls and the boundaries of circular discs. For a straight wall section  $\gamma_r = 0$  and for a disc of radius  $r$  we have  $\gamma_r = \pm \frac{1}{r}$ , with  $-$  for collisions happening from the inside of the disc (as in the MB) and  $+$  otherwise (as in the PSB). Here  $\mathbf{n}$  denotes the normal vector of the boundary segment at the collision point  $\mathbf{q}$ , and  $\phi$  is the angle of incidence. The vectors  $\mathbf{e}, \mathbf{e}'$  are unit vectors orthogonal to the incident and reflected momenta  $\mathbf{p}$  and  $\mathbf{p}'$  respectively (for more details see [23]).

Notice that a collision with a straight wall does not change the norm of  $\delta\mathbf{\Gamma}$  because both the coordinate and the velocity components are reflected specularly.

### B. With magnetic field

We now extend the DPH formalism for a particle experiencing a magnetic field perpendicular to the billiard plane. In this section we present only the final expressions. The full calculations are presented in appendix A.

The free evolution of the perturbation vector  $\delta\mathbf{\Gamma}(t)$  in

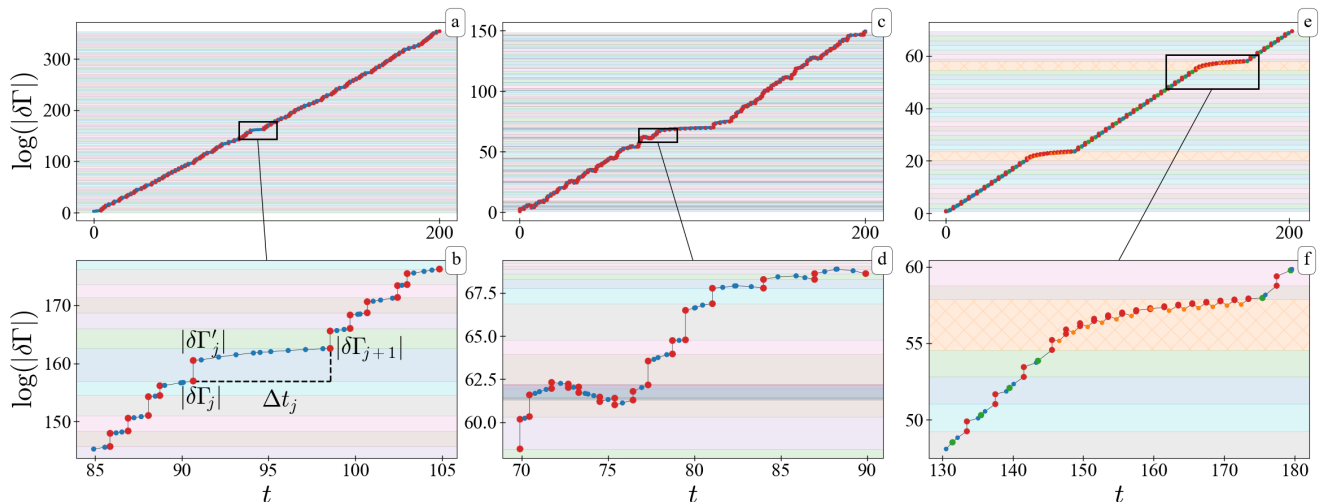


FIG. 2. Typical time evolution of the logarithm of the norm of the perturbation vector  $|\delta\Gamma(t)|$  for the periodic Sinai billiard without (a) and with (c) magnetic field ( $B = 1$ ) and for the mushroom billiard (e). Zoom-ins are below each panel. For (a-d) red markers mean collision with the disc while blue markers mean “collision” with the periodic walls (not a true collision, but a way of recording the value of  $|\delta\Gamma|$ ). For (e-f) red is collision with cap head, orange with cap walls, blue with stem sides and green with stem bottom. The coloured background stripes denote the unit cells (random colors are used) with hatched orange color used for the laminar phases.

the presence of a perpendicular magnetic field is given by

$$\delta\Gamma(t) = \mathbb{B} \cdot \delta\Gamma(t_0), \quad (7)$$

$$\mathbb{B} = \begin{pmatrix} \mathbb{I}_{2 \times 2} & \begin{matrix} \rho \sin(\omega t) & \rho (\cos(\omega t) - 1) \\ -\rho (\cos(\omega t) - 1) & \rho \sin(\omega t) \end{matrix} \\ 0_{2 \times 2} & \begin{matrix} \cos(\omega t) & -\sin(\omega t) \\ \sin(\omega t) & \cos(\omega t) \end{matrix} \end{pmatrix}$$

with the cyclotron frequency  $\omega = 2B$  and the cyclotron radius  $\rho = 1/\omega$ . In the billiard the particle always moves with unit velocity by convention. The expressions that give the discontinuous change of the perturbation vector at a collision with a wall or disc are

$$\delta\Gamma' = \begin{pmatrix} \delta\mathbf{q} - 2(\delta\mathbf{q} \cdot \mathbf{n}) \mathbf{n} \\ \delta\mathbf{p} - 2(\delta\mathbf{p} \cdot \mathbf{n}) \mathbf{n} - 2\gamma_r \frac{\langle \delta\mathbf{q}, \mathbf{e} \rangle}{\cos\phi} \mathbf{e}' \end{pmatrix} - \omega \frac{(\delta\mathbf{q} \cdot \mathbf{n})}{(\mathbf{p} \cdot \mathbf{n})} \begin{pmatrix} 0 \\ \mathbb{S} \cdot \mathbf{p} \end{pmatrix} \quad (8)$$

$$\mathbb{S} = 2 \begin{pmatrix} -2n_1 n_2 & n_1^2 - n_2^2 \\ n_1^2 - n_2^2 & 2n_1 n_2 \end{pmatrix}, \quad \mathbf{n} = \begin{pmatrix} n_1 \\ n_2 \end{pmatrix}$$

where  $\gamma_r$  again is the curvature of the wall segment (0 for a straight wall,  $\pm\frac{1}{r}$  for a disc).

### C. The “toy model”

Before finding an approximate expression for the value of  $\lambda$  in our model systems, it is worthwhile to get an impression of how the norm of the perturbation vector evolves with time. In Fig. 2 we show typical plots for

the three different billiards. We computed the perturbation growth using the DPH framework, sampling the perturbation vector immediately before and after every collision to resolve the instantaneous jumps. As the DPH evolution is linear, in the actual numerical simulations we renormalized the perturbation vector after sampling to prevent numerical error due to the rapid perturbation growth.

Let us first examine Fig. 2(a, b). We see that the norm of the perturbation vector changes in two ways. Let the  $j$ -th collision with a disc happen at time  $t_j = \sum_{i=0}^{j-1} \Delta t_i = t_{j-1} + \Delta t_{j-1}$ . There a discontinuous change of the perturbation vector norm happens, so that  $|\delta\Gamma'_j| = a_j |\delta\Gamma_j|$  (in general  $a_j$  is a function of  $\delta\Gamma_j$ ). The collision event is followed by a time-interval  $\Delta t_j$ , in which the perturbation norm changes continuously because there are no collisions with curved boundaries. Just before the next collision with a disc the perturbation norm takes the value  $|\delta\Gamma_{j+1}|$ . In the following we will refer to this segment of the growth curve as a *unit cell*, starting with one collision event with a disc and ending just before the next one.

A crucial simplification we do in deriving an approximate expression for the Lyapunov exponent will be to express the perturbation growth in the time-interval  $\Delta t_j$  as a function  $z(\Delta t_j)$  of the interval length. The actual precise value  $|\delta\Gamma_{j+1}|/|\delta\Gamma'_j|$  is not a simple scalar function of the time interval since for example in the case of the PSB we can obtain from Eq. (5)

$$|\delta\Gamma_{j+1}(\Delta t)| = \sqrt{(\delta\mathbf{q}'_j + \delta\mathbf{p}'_j \Delta t)^2 + (\delta\mathbf{p}'_j)^2} \quad (9)$$

(due to the linearity of the equations of motion of the

tangent space we can assume a norm of  $|\delta\Gamma'_j| = 1$  in Eq. (9). Eq. (9) depends on the initial orientations of both the momentum and position deviation vectors and thus is not a function of just  $\Delta t$ .

We will show, however, by analysing numerical data, that a reasonable approximation can be obtained by assuming that such a function  $z(\Delta t)$  exists. For each unit cell we thus write

$$|\delta\Gamma_{j+1}| = z(\Delta t_j) \times a_j \times |\delta\Gamma_j| = z(\Delta t_j) \times |\delta\Gamma'_j|. \quad (10)$$

We then recursively apply Eq. (10) to get

$$\begin{aligned} |\delta\Gamma_n| &= \prod_{i=0}^{n-1} a_i z(\Delta t_i) |\delta\Gamma(0)| \Rightarrow \\ \log(|\delta\Gamma_n|) &= \sum_{i=0}^{n-1} \log(a_i) + \log(z(\Delta t_i)) \end{aligned} \quad (11)$$

(using  $|\delta\Gamma(0)| = 1$ ) and with  $T_n = \sum_{i=0}^{n-1} \Delta t_i$  we use Eq. (4) to write  $\lambda = \lim_{n \rightarrow \infty} \log(|\delta\Gamma_n|)/T_n$ . The quotient of the infinite sums is the same as the ratio of the average over all unit cells (denoted by  $\langle \cdot \rangle$ ), i.e.

$$\lambda \approx \frac{1}{\kappa} (\langle \log(a) \rangle + \langle \log(z(\Delta t)) \rangle) \quad (12)$$

$$\kappa \equiv \langle \Delta t \rangle. \quad (13)$$

For the billiards considered here we have found that furthermore  $\langle \log(z(\Delta t)) \rangle = \log(z(\langle \Delta t \rangle)) = \log(z(\kappa))$  is a good approximation that we will use.

In the remainder of the text we will call Eq. (12) the ‘‘toy model’’. It is the more detailed version of the back-of-the-envelope calculation given in the introduction, i.e.  $C = \langle a \times z(\Delta t) \rangle$ . In the following sections we will apply this toy model to specific billiards and see how well it approximates the Lyapunov exponent and its parameter dependence.

#### D. Software

All numerical computations presented in this paper were performed with an open source software to simulate billiards, **DynamicalBilliards.jl** [29]. The software also has implemented the DPH framework for computing  $\lambda$ , as well as its extension for magnetic fields.

### III. RESULTS

#### A. Periodic Sinai billiard

We start our analysis with the PSB because it is the simplest case and we are able to give a fully analytical expression for the Lyapunov exponent in the simplified toy model. We note that in the absence of a magnetic field the PSB is ergodic and its phase space is not mixed.

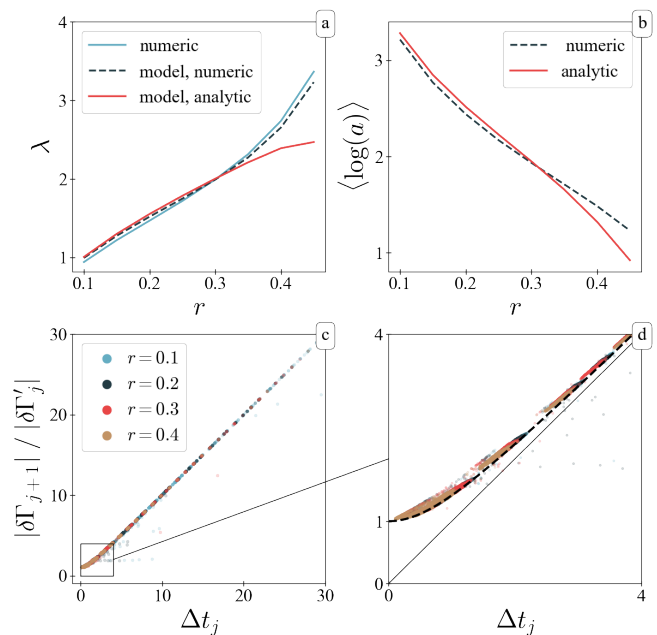


FIG. 3. (a) Lyapunov exponent of the periodic Sinai billiard for different radii, compared with the toy model. The dashed curve obtains  $\langle \log(a) \rangle$  by numeric average while the red curve uses Eq. (19). The blue curve is using the DPH framework. (b) Average value of  $\langle \log(a) \rangle$  used in panel (a). (c) Perturbation norm increase during the free flight part. In the zoom in (d) we also plot the curve  $\sqrt{1 + \Delta t^2}$  as a dashed line.

Nevertheless, it will serve as a pedagogic example of how the toy model approximates the Lyapunov exponent.

For the PSB  $\tau = \kappa$  and the value of  $\tau$  is known from Eq. (3)

$$\kappa_{\text{PSB}} = \frac{1 - \pi r^2}{2r}. \quad (14)$$

An approximation for  $z(\Delta t)$  is easily found as well from Eq. (9), namely

$$z_{\text{PSB}}(t) \approx \sqrt{1 + t^2} \quad (15)$$

which uses the assumption that after a collision with a disc the momentum contribution to the perturbation vector is much larger than the position contribution, i.e.  $|\delta\mathbf{p}'| \gg |\delta\mathbf{q}'|$ . Numerical calculations show that this approximation is valid for small enough radii (see Fig. 3). The instantaneous change factor  $\langle \log(a) \rangle$  is rather large for all but very large disc radii. Also as seen in panel (c) and its inset (d), Eq. (15) almost perfectly approximates the perturbation norm increase during the free flight part.

We still need an approximate expression for  $a$ , the instantaneous change factor, which we can derive from Eq. (6). Since the norm of the position deviation does not change at the collision, we focus on the momentum deviation  $\delta\mathbf{p}' = \delta\mathbf{p}^{(r)} - \frac{2}{r} \frac{\delta\mathbf{q} \cdot \mathbf{e}}{\cos(\theta)} \mathbf{e}'$  with  $\delta\mathbf{p}^{(r)} = \delta\mathbf{p} - 2(\delta\mathbf{p} \cdot \mathbf{n}) \mathbf{n}$

(if not explicitly written otherwise all quantities in this paragraph have a collision-time index  $j$ , which we suppress to make the symbols simpler). We define  $A = \frac{2}{r} \frac{\delta \mathbf{q} \cdot \mathbf{e}}{\cos(\phi)}$  and carrying out the calculations leads to

$$|\delta \Gamma'|/|\delta \Gamma| = a = \sqrt{1 + A^2 - 2A(\mathbf{e}' \cdot \delta \mathbf{p})} \quad (16)$$

again using the assumption that  $|\delta \Gamma_j| = 1$  (and recall that  $|\delta \mathbf{p}^{(r)}| = |\delta \mathbf{p}|$ ,  $|\delta \mathbf{q}'| = |\delta \mathbf{q}|$ ).

We now need to average  $\langle \log(a) \rangle$ . We start our approximation by replacing the inner product  $(\delta \mathbf{q} \cdot \mathbf{e})$  by an averaged quantity  $b(r)$  (we show below how  $b$  depends on  $r$ ). It is expected that perturbations will grow and orient themselves perpendicular to the particle's direction of motion. Since  $\mathbf{e}$  is a unit vector perpendicular to the particle's momentum and thus parallel to  $\delta \mathbf{q}$ , this means that  $\langle |(\delta \mathbf{q} \cdot \mathbf{e})|/|\delta \Gamma| \rangle = \langle |\delta \mathbf{q}|/|\delta \Gamma| \rangle = b(r)$ .

Which portion of  $|\delta \Gamma|$  is contained in  $|\delta \mathbf{q}|$  is answered based on how perturbations evolve during the free flight part. Starting from the  $j$ -th collision the perturbations evolve for time  $\Delta t_j$ . Using Eq. (9) (and assuming that the cross-terms  $\delta \mathbf{p} \cdot \delta \mathbf{q}$  will drop out in the averaging) we obtain

$$\frac{|\delta \mathbf{q}_{j+1}|}{|\delta \Gamma_{j+1}|} = \frac{\sqrt{\frac{|\delta \mathbf{q}'_j|^2}{|\delta \mathbf{p}'_j|^2} + \Delta t_j^2}}{\sqrt{\frac{|\delta \mathbf{q}'_j|^2}{|\delta \mathbf{p}'_j|^2} + 1 + \Delta t_j^2}}. \quad (17)$$

To analytically resolve eq. (17) we use the same assumption as in eq. (15),  $|\delta \mathbf{p}'| \gg |\delta \mathbf{q}'|$ . We then average, replacing  $\Delta t$  by  $\kappa$ , which leads to

$$b(r) = \sqrt{\frac{\kappa_{\text{PSB}}^2}{1 + \kappa_{\text{PSB}}^2}}. \quad (18)$$

We discard the term  $2A(\mathbf{e}' \cdot \delta \mathbf{p})$  in Eq. (16) again assuming that the inner product averages to 0. Now the only variable left to average over is  $\phi$ , the angle with respect to the normal vector. This is distributed in  $[-\pi/2, \pi/2]$  with probability distribution of  $\cos(\phi)/2$ . Therefore

$$\begin{aligned} \langle \log(a) \rangle &= \int_{-\pi/2}^{\pi/2} \log \left( \sqrt{1 + \left( \frac{2b}{r \cos(\phi)} \right)^2} \right) \frac{\cos(\phi)}{2} d\phi \\ &= \frac{\text{csch}^{-1} \left( \frac{2b}{r} \right) \sqrt{4b^2 + r^2}}{r} + \log \left( \frac{b}{r} \right) \end{aligned} \quad (19)$$

with  $\text{csch}^{-1}$  the inverse hyperbolic cosecant.

We then put eqs. (14), (15), (18) and (19) into the toy model of Eq. (12) and obtain an analytic approximation

for the Lyapunov exponent

$$\lambda_{\text{PSB}}(r) = \frac{2r}{1 - \pi r^2} \left( \frac{\text{csch}^{-1} \left( \frac{2b(r)}{r} \right) \sqrt{4b(r)^2 + r^2}}{r} + \log \left( \frac{b(r)}{r} \right) + \log \left( \sqrt{1 + \left( \frac{1 - \pi r^2}{2r} \right)^2} \right) \right). \quad (20)$$

The result is shown in Fig. 3(a), compared with the numerical value of  $\lambda$  using the DPH framework as well as with the result of computing the term  $\langle \log(a) \rangle$  in the toy model numerically from the evolution of the perturbation vector norm. All three curves are in excellent agreement for small and intermediate  $r$ , only for large  $r$  does Eq. (20) slightly deviate from the numerical values because the approximation for  $b(r)$  in Eq. (18) and thus for  $\langle \log(a) \rangle$  becomes less accurate.

## B. Magnetic periodic Sinai billiard

We now want to apply the same process to the MPSB, which, however, has a mixed phase space: there exist collision-less orbits like those seen in Fig. 1(b) that constitute the regular part of phase space. We are of course only considering the Lyapunov exponent of the chaotic part of the phase space, which means that we initialise particles only in the chaotic phase space region. The mean collision time between discs ( $\kappa_{\text{MPSB}}$  below) is also only defined for the chaotic phase space part (as the regular trajectories do not collide with the discs).

The free flight evolution in the MPSB is fundamentally different from the PSB. Not only are the functional forms different but in addition due to magnetic focusing it is possible (and in fact quite frequent) for the perturbation norm to *decrease* during the evolution, as can be seen in Fig. 4(e,f). In addition, as visible in Fig. 2(d), it is also possible for the norm to decrease during the instantaneous change as well.

This more complex behaviour is of course hidden in the more complicated formulas of our extension to the DPH framework for magnetic fields. For example, explicitly writing out Eq. (7) gives

$$\begin{aligned} |\delta \Gamma(t)| &= \left[ (\delta p_x^2 + \delta p_y^2) + \left( \delta q_x + \delta p_y \frac{\cos(\omega t) - 1}{\omega} + \delta p_x \frac{\sin(\omega t)}{\omega} \right)^2 + \left( \delta q_y - \delta p_x \frac{\cos(\omega t) - 1}{\omega} + \delta p_y \frac{\sin(\omega t)}{\omega} \right)^2 \right]^{1/2} \end{aligned} \quad (21)$$

(where again we assumed  $|\delta \Gamma(0)| = 1$ ). The consequences of Eq. (21) can be seen in Fig. 4(d, e). Using a uni-variate scalar function  $z(\Delta t)$  to approximate these distributions

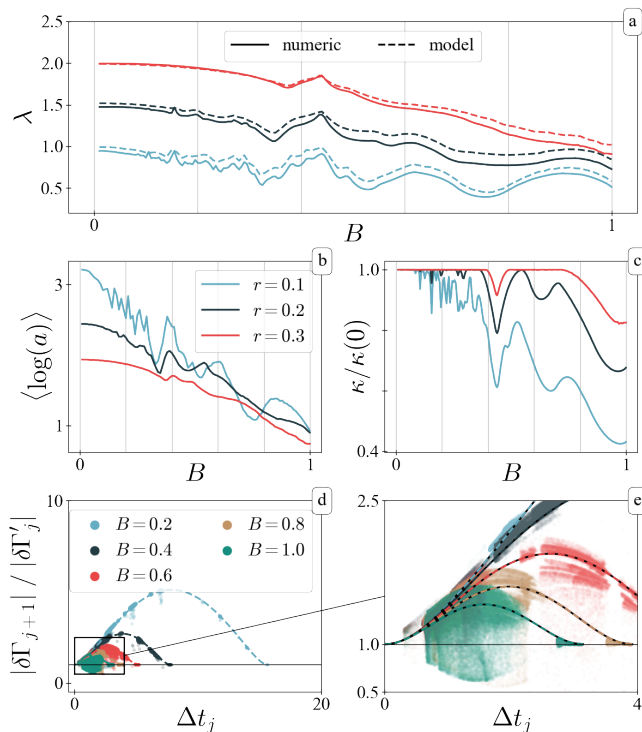


FIG. 4. (a) Lyapunov exponent of the magnetic periodic Sinai billiard (MPSB) for different radii versus the magnetic field, compared with the toy model. The solid curves are the numeric result  $\lambda$ , the dashed curves are the toy model using  $\langle \log(a) \rangle$ . (b) Numeric average of  $\log(a)$  versus the magnetic field. (c) Chaotic phase space portion ( $g_c = \kappa/\kappa(0)$ ) of the MPSB ((a-c) share legend). (d, e) Perturbation norm change during the free flight in the MPSB. Plotted with dashed lines are Eq. (22) (data for  $r = 0.2$ ).

appears to be a bold move, but in the end it will turn out to give a good approximation. To obtain  $z(\Delta t)$  we simplify Eq. (21) to

$$z_{\text{MPSB}}(t) = \sqrt{1 + \left(\frac{1 - \cos(\omega t)}{\omega}\right)^2 + \left(\frac{\sin(\omega t)}{\omega}\right)^2}. \quad (22)$$

which is also plotted in Fig. 4(d, e).

In the next step we compute  $\langle \log(a) \rangle$  numerically and use its value in the toy model along with  $z_{\text{MPSB}}(\kappa(B))$ . We remind that the value of  $\kappa$ , the mean collision time between discs in MPSB, is not known analytically but it is connected with the chaotic phase space portion through Eq. (1). The results of the toy model are presented in Fig. 4.

Besides the fact that our toy model approximates  $\lambda$  very accurately, Fig. 4 nicely shows the impact of phase space restriction on  $\lambda$ . In our toy model the value of  $\lambda$  is composed of five contributions, the first being the denominator  $\kappa$ . The value of  $\langle \log(a) \rangle$  itself has two contributions, one again stemming from  $\kappa$  (as shown in the previous section) and the other from  $B$ . The function  $z_{\text{MPSB}}$  also has two contributions, one from  $B$  and one

from  $\kappa$ . Therefore three out of five contributions to  $\lambda$  are inherently linked to the restriction of the chaotic phase space by regular orbits.

### C. Mushroom billiard

Because the volume fractions of the regular and the chaotic phase space regions are not known analytically in the MPSB we have turned to a billiard that also has a mixed phase space but allows to calculate this fractions, and, as we will show, the relevant average time scales analytically: the mushroom billiard (MB). The regular orbits in the MB are orbits forever staying in the cap, evolving exactly like they would as if they were in a circular billiard [30]. The tangential circle to these orbits has a radius  $\geq w/2$  as shown in Fig. 1(a). The rest of the orbits, which do not satisfy this criterion, eventually enter the stem and are chaotic. The tangential circle argument was used in [5] to obtain an analytic expression for the regular phase space volume  $V_{\text{REG}}$  of the MB as a function of the billiard parameters

$$V_{\text{REG}} = 2\pi \left( \arccos\left(\frac{w}{2}\right) - \frac{w}{2} \left(1 - \frac{w^2}{4}\right) \right) \quad (23)$$

$$V_{\text{TOT}} = 2\pi(hw + \pi/2), \quad (24)$$

where  $V_{\text{TOT}}$  is the parameter dependence of the total phase space volume (all lengths are scaled to the cap radius  $r$  which therefore is fixed to  $r = 1$ ). We then obtain the chaotic phase space portion as  $g_c = 1 - V_{\text{REG}}/V_{\text{TOT}}$ , which we plot in Fig. 5(c,d). Interestingly,  $g_c$  does not appear to vanish for small  $h$ , although it is obvious that there are no chaotic orbits for  $h = 0$ . This discontinuity is due to the fact that the volume of chaotic phase space in the cap is independent of stem height for nonzero  $h$ , but drops to zero for  $h = 0$ .

In Fig. 6(c,d) we present a scatter plot of various possible increases of the perturbation norm during the unit cells. We found that there are clearly distinct contributions to the increase, each seemingly approximated as linear function of  $\Delta t$ . By analysing the dynamics in more detail, it turns out that the different contributions of Fig. 6(c,d) come from the trapping of the chaotic orbits in the regular phase space. In coordinate space this means that the particles get trapped in the cap and mimic the motion of the regular phase space there until eventually escaping after some time. This effect is often called *intermittency*, and is known to occur in mushroom billiards [31, 32].

We therefore have to separate the unit cell into two different “episodes”: the chaotic episode  $c$  and the laminar episode  $\ell$ , where the particle is trapped in the cap. We show these episodes in Fig. 5(a). Numeric calculations shown in Fig. 6(e, f) show that each episode has a different average time,  $\tau_c, \tau_\ell$  respectively.

During the chaotic episodes the picture is very similar to the PSB. A collision with the cap head gives an

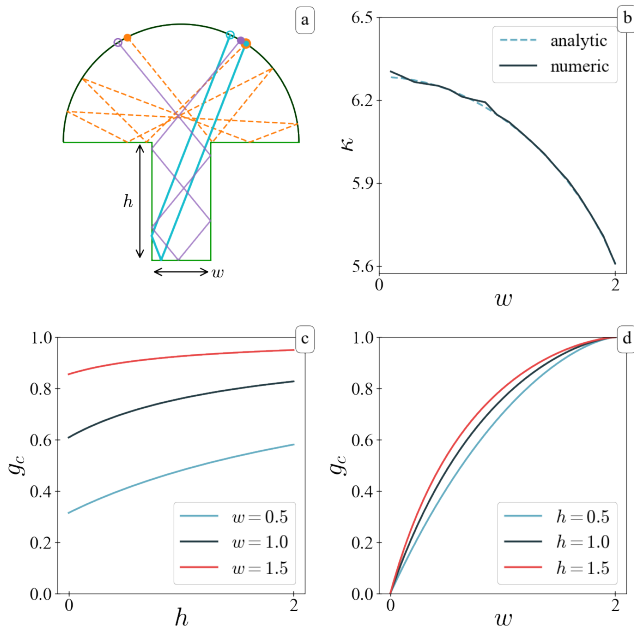


FIG. 5. (a) A laminar episode (orange, dashed) and two chaotic episodes (blue, purple) in the mushroom billiard. Starts and ends of each episode are denoted with closed and open circles and the blue episode starts directly after the orange. The cap head is plotted in dark color to differentiate. (b) Mean return time to the stem bottom, which is equivalent with the average unit cell time, eqs. (26), (27). (c,d) Portion of chaotic phase space for the mushroom billiard.

instantaneous increase to  $|\delta\Gamma|$ , followed by an approximately linear increase until the next collision with the cap head. Here the linear increase approximation is valid because for the chaotic episodes  $\Delta t \gtrsim 2h + 2 - w$ . After colliding with the cap head the particle may return to the stem immediately which initialises another chaotic episode. Occasionally, after ending a chaotic episode, the particle will get trapped in the cap (see Fig. 5(a) orange), starting a laminar episode. Even though there are successive collisions with the cap head in this episode, the perturbations do not increase exponentially. The successive instantaneous increases are very quickly becoming insignificant (see Fig. 2(e,f)) due to the fact that cap collisions have an initially focusing effect which only becomes de-focusing if the consecutive free motion is long enough, which is not the case in the laminar episodes. Therefore the overall perturbation growth inside the cap trapping episodes is *linear*.

Let  $n_c$  and  $n_\ell$  be the counts of chaotic and laminar episodes up to time  $T$ . Notice that  $n_\ell$  is strictly less than  $n_c$  since a chaotic episode always follows a laminar episode, but the inverse is only occasionally true. In the limit  $T \rightarrow \infty$  we define  $f_\ell = n_\ell / (n_\ell + n_c)$  to be the frequency of the laminar episodes. We then write the function  $z$  as

$$z_{\text{MB}}(\Delta t) = (o_c + s_c \Delta t_c) + f_\ell (o_\ell + s_\ell \Delta t_\ell) \quad (25)$$

with  $o_i$  the offset and  $s_i$  the slope of the linear approximation (we obtain these values with least squares fit to Fig. 6(c, d)). For the chaotic episodes  $s, o$  are constant versus  $h, w$  while for the laminar episodes  $o$  depends strongly on  $w$ . Also, for the chaotic episodes  $o$  has negative value (of around -0.8) which is expected due to the focusing effect. We once again compute  $\langle \log(z(\Delta t)) \rangle$  simply by replacing  $\Delta t$  by its average values  $\tau_c, \tau_\ell$  in Eq. (25).

The instantaneous change factor  $a$  is the same between the laminar and chaotic episodes so we do not need to separate it. Notice that for the laminar episode we only consider the first jump as the instantaneous increase. Subsequent jumps that decrease rapidly are encoded in the linear growth approximation. After computing  $\langle \log(a) \rangle$  numerically, we still need a value for  $\kappa_{\text{MB}}$ , the unit cell average time, to apply our toy model  $\lambda = (\langle \log(a) \rangle + \log(z_{\text{MB}}(\tau_c, \tau_\ell))) / \kappa_{\text{MB}}$ . Numerically we can estimate

$$\kappa_{\text{MB}} = \tau_c + f_\ell \tau_\ell. \quad (26)$$

However we can estimate  $\kappa_{\text{MB}}$  analytically as well, using Kac's lemma [33–35]. The key to this is understanding that the mean cell time is equivalent with the mean return time to the stem bottom, since all phases in the end of the day have to go there, since all phases are part of the chaotic phase space.

We present the full proof in appendix B. The final expression is given by

$$\kappa_{\text{MB}}(h, w) = g_c(h, w) \frac{\pi(hw + \pi/2)}{w} \quad (27)$$

with  $g_c$  here being the portion of chaotic phase space of the MB. We compare the analytic formula with the numeric result in Fig. 5(b) and find the expected perfect agreement, since Eq. (27) is exact. In appendix C we also present an analytic approximation for  $\tau_c$ . Since we know  $\kappa_{\text{MB}}$  and  $\tau_c$  analytically, we also know the product  $f_\ell \tau_\ell$  (but we don't have an expression for  $f_\ell$  or  $\tau_\ell$  individually).

We can now use our toy model to compare with  $\lambda$ , which we do in Fig. 6(a, b). Again we find good agreement between toy model and the numerical simulation using the DPH framework. The model mildly diverges for very small  $w$ , probably because the mean laminar time  $\tau_\ell$  diverges as seen in Fig. 6(e).

As was the case in the MPSB, the average unit cell time  $\kappa$  is inversely proportional to  $\lambda$  and directly proportional to the chaotic phase space portion  $g_c$ . This shows that phase space restrictions have an immediate impact in the value of the Lyapunov exponent even for billiards with intermittent dynamics. Notice that in the MB both  $g_c$  and  $\lambda$  increase as  $w$  increases. This is for two reasons; firstly  $\kappa$  depends on the chaotic phase space *volume* and not just the relative proportion. The total volume of the MB changes with  $w$  (which is not the case in the MPSB: the total volume is independent of  $B$ ). Secondly, it happens here that besides  $g_c$  there are also other factors that depend on  $w$  in Eq. (27), which was not the case in Eq. (1) for the MPSB.

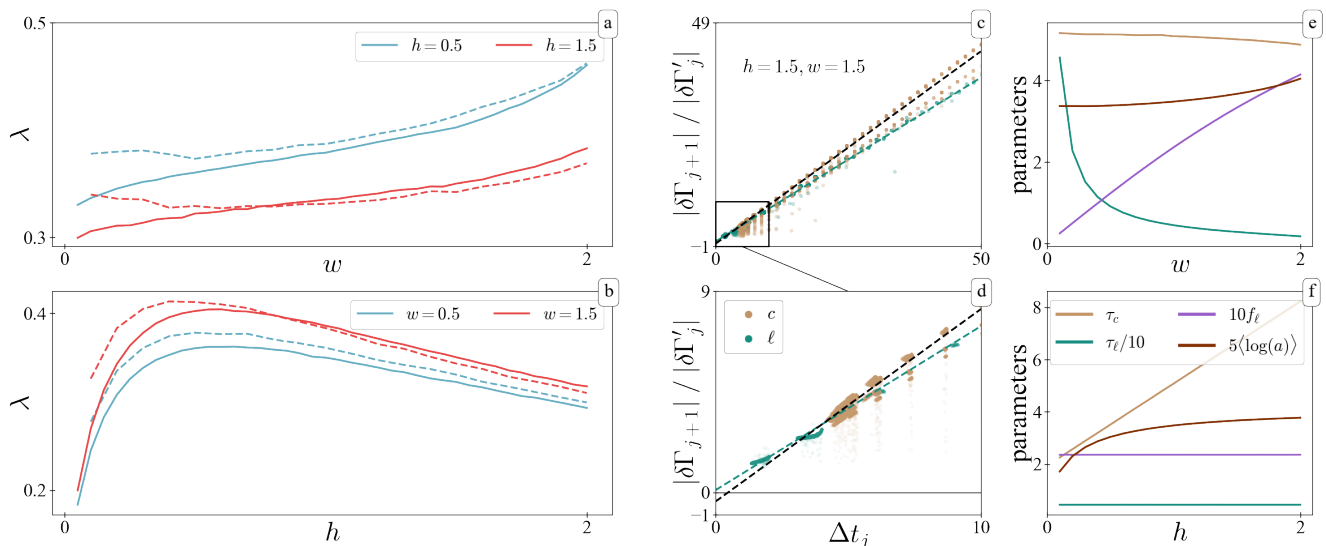


FIG. 6. (a, b) Lyapunov exponents in the mushroom billiard (MB) versus the width  $w$  or height  $h$  of the stem. Solid lines are numeric results using the DPH framework, dashed lines are using the toy model. (c, d) Perturbation norm increase during the chaotic  $c$  and laminar  $\ell$  episodes. (e, f) Parameters of the toy model versus  $w$  or  $h$  (for constant  $h = 1$  and  $w = 1$  respectively); legend is shared.

#### IV. CONCLUSIONS

To summarise, we have examined the value of the Lyapunov exponent  $\lambda$  in chaotic billiards. We were able to create a conceptually simple model that approximates  $\lambda$  very well. The model is based on how perturbations evolve in billiards *on average* and helps to understand how each part of the dynamics contributes to the perturbation increase. The simple model is written as

$$\lambda = \frac{1}{\kappa} (\langle \log(a) \rangle + \langle \log(z(\Delta t)) \rangle) \quad (28)$$

where  $a$  the instantaneous change of  $|\delta\mathbf{\Gamma}|$  at a collision with a curved boundary and  $z(t)$  the continuous change of  $|\delta\mathbf{\Gamma}|$  in between collisions with curved boundaries.  $\kappa$  is the average unit cell time equal to the mean collision time between curved boundaries. We believe Eq. (28) is a valid approximation for  $\lambda$  for generic chaotic billiards. Furthermore, for the billiards considered here we found that  $\langle \log(z(\Delta t)) \rangle \approx \log(z(\kappa))$  is a good approximation as well.

We used Eq. (28) to find an analytic expression for  $\lambda$  in the PSB. We have also shown that this simplified expression can closely replicate the numerically exact values of  $\lambda$  in the MPSB. We could follow the same approach for the MB, even though the process is complicated in this case by intermittent dynamics. In both billiards with mixed phase space we were able to connect the chaotic phase space portion with  $\lambda$  through  $\kappa$ . Due to the generality of Kac's lemma, we believe this connection to be universal. Thus in conclusion we see that  $\lambda$  is in general roughly inversely proportional to the chaotic phase space portion, allowing an estimation of the Lyapunov

exponent and its parameter dependence in mixed phase space systems. We have seen, however, that in a more detailed analysis  $\kappa$  and thus the phase space fractions additionally enter the collision term  $\langle \log(a) \rangle$  and that magnetic focusing and intermittency can lead to additional corrections to the Lyapunov exponent.

#### Appendix A: Evolution of perturbation vector in a magnetic field

In their paper, Dellago, Posch and Hoover give two main equations to compute the evolution of perturbations in tangent space along a piece-wise smooth flow defined by the autonomous ODE system

$$\dot{\mathbf{\Gamma}} = \mathbf{F}(\mathbf{\Gamma}). \quad (A1)$$

During smooth propagation, the perturbation vector  $\delta\mathbf{\Gamma}$  along the trajectory  $\mathbf{\Gamma}$  evolves according to

$$\delta\dot{\mathbf{\Gamma}} = \left. \frac{\partial \mathbf{F}}{\partial \mathbf{\Gamma}} \right|_{\mathbf{\Gamma}} \cdot \delta\mathbf{\Gamma}. \quad (A2)$$

If smooth propagation is interrupted at discrete times  $t_j(\mathbf{\Gamma})$  by a discontinuous jump, represented here by a differentiable map  $\mathbf{M}_j(\mathbf{\Gamma})$ , the perturbation vector after the jump is given by

$$\delta\mathbf{\Gamma}' = \left. \frac{\partial \mathbf{M}_j}{\partial \mathbf{\Gamma}} \right|_{\mathbf{\Gamma}} \cdot \delta\mathbf{\Gamma}_i + \left( \left. \frac{\partial \mathbf{M}_j}{\partial \mathbf{\Gamma}} \right|_{\mathbf{\Gamma}} \cdot \mathbf{F}(\mathbf{\Gamma}_i) - \mathbf{F}(\mathbf{M}(\mathbf{\Gamma})) \right) \delta\tau_c \quad (A3)$$

where  $\delta\tau_c = t_j(\mathbf{\Gamma} + \delta\mathbf{\Gamma}) - t_j(\mathbf{\Gamma})$ . For the case of elastic reflection with an obstacle,  $\mathbf{M}_j$  can be written as

$$\mathbf{\Gamma}' = \mathbf{M}_j(\mathbf{\Gamma}) = \left( \begin{array}{c|c} \mathbb{I}_{2 \times 2} & \mathbf{0}_{2 \times 2} \\ \hline \mathbf{0}_{2 \times 2} & \mathbb{I}_{2 \times 2} - 2(\mathbf{n} \otimes \mathbf{n}) \end{array} \right) \cdot \mathbf{\Gamma}. \quad (\text{A4})$$

Here  $\mathbf{n}$  is the normal vector of the obstacle at the collision point,  $\mathbb{I}_{2 \times 2}$  and  $\mathbf{0}_{2 \times 2}$  are the  $2 \times 2$  identity and zero matrices respectively, and  $(\mathbf{a} \otimes \mathbf{b})_{jk} = a_j b_k$  is a second-order tensor.

### 1. Propagation

In magnetic billiards, particles propagate in circular arcs. To get the simplest possible set of equations of motion describing this mode of propagation, it is useful to introduce a phase angle  $\theta = \arctan(p_y/p_x)$ . For uniform circular motion, this phase angle grows linearly in time as the system rotates with constant angular velocity  $\omega$ . This can be exploited to determine  $\dot{\mathbf{p}}$  using the chain rule

$$\dot{\mathbf{p}} = \frac{d\mathbf{p}}{dt} = \frac{d\theta}{dt} \cdot \frac{d\mathbf{p}}{d\theta} = \omega \cdot \frac{d\mathbf{p}}{d\theta}. \quad (\text{A5})$$

Using  $\|\mathbf{p}\| = 1$ , one can easily calculate the explicit relation between  $\mathbf{p}$  and  $\theta$

$$\begin{aligned} p_x = \cos(\theta) & \Rightarrow \frac{dp_x}{d\theta} = -p_y \\ p_y = \sin(\theta) & \Rightarrow \frac{dp_y}{d\theta} = p_x \end{aligned} \quad (\text{A6})$$

and combine the results of eqs. (A5) and (A6) to receive the equations of motion

$$\mathbf{F}(\mathbf{\Gamma}) = \begin{pmatrix} \mathbf{p} \\ \omega \cdot \mathbf{R} \mathbf{p} \end{pmatrix} \quad \text{where } \mathbf{R} = \begin{pmatrix} 0 & -1 \\ 1 & 0 \end{pmatrix}. \quad (\text{A7})$$

Using Eq. (A2), we can now state the equations of evolution for a perturbation vector  $\delta\mathbf{\Gamma}$  using the Jacobian  $\mathbf{J}$  of  $\mathbf{F}$ .

$$\delta\dot{\mathbf{\Gamma}} = \mathbf{J} \cdot \delta\mathbf{\Gamma} = \left( \begin{array}{c|c} \mathbf{0}_{2 \times 2} & \mathbb{I}_{2 \times 2} \\ \hline \mathbf{0}_{2 \times 2} & -\omega \cdot \mathbf{R} \end{array} \right) \delta\mathbf{\Gamma}. \quad (\text{A8})$$

Using an exponential ansatz, we can compute the general solution of this system and receive a final result of

$$\delta\mathbf{\Gamma}(t) = \mathbb{B} \cdot \delta\mathbf{\Gamma}(t_0), \quad (\text{A9})$$

$$\mathbb{B} = \left( \begin{array}{c|cc} \mathbb{I}_{2 \times 2} & \rho \sin(\omega t) & \rho (\cos(\omega t) - 1) \\ \hline \mathbf{0}_{2 \times 2} & -\rho (\cos(\omega t) - 1) & \rho \sin(\omega t) \\ \hline & \cos(\omega t) & -\sin(\omega t) \\ & \sin(\omega t) & \cos(\omega t) \end{array} \right)$$

where  $\rho = 1/\omega$  is the cyclotron radius.

### 2. Collisions

The derivation of the collision map for  $\delta\mathbf{\Gamma}$  is largely analogous to the process used by DPH to derive their result for non-magnetic billiards. The equations of motion are assumed as stated in Eq. (A7). For equation (A3), we require the Jacobian matrix of  $\mathbf{M}_j$ , which is

$$\frac{\partial \mathbf{M}_j}{\partial \mathbf{\Gamma}} = \begin{pmatrix} \mathbb{I}_{2 \times 2} & \mathbf{0} \\ \mathbf{A} & \mathbf{B} \end{pmatrix} \quad (\text{A10})$$

$$\begin{aligned} \text{where } \mathbf{A} &= 2((\mathbf{n} \otimes \mathbf{p}) + \langle \mathbf{p}, \mathbf{n} \rangle \mathbb{I}_{2 \times 2}) \frac{\partial \mathbf{n}}{\partial \mathbf{q}} \\ \mathbf{B} &= \mathbb{I}_{2 \times 2} - 2(\mathbf{n} \otimes \mathbf{n}). \end{aligned}$$

By inserting eqs. (A7), (A4) and (A10) into (A3), we find

$$\begin{aligned} \delta\mathbf{\Gamma}' &= \begin{pmatrix} \mathbb{I}_{2 \times 2} & \mathbf{0} \\ \mathbf{A} & \mathbf{B} \end{pmatrix} \delta\mathbf{\Gamma} + \left[ \begin{pmatrix} \mathbb{I}_{2 \times 2} & \mathbf{0} \\ \mathbf{A} & \mathbf{B} \end{pmatrix} \cdot \right. \\ &\quad \left. \begin{pmatrix} \mathbf{p} \\ \omega \cdot \mathbf{R} \mathbf{p} \end{pmatrix} - \begin{pmatrix} \mathbf{p} - 2(\mathbf{n} \otimes \mathbf{n}) \mathbf{p} \\ \omega \cdot \mathbf{R} \mathbf{B} \mathbf{p} \end{pmatrix} \right] \delta\tau_c. \end{aligned} \quad (\text{A11})$$

It is now helpful to continue calculations for  $\delta\mathbf{q}'$  and  $\delta\mathbf{p}'$  separately. For the position component  $\delta\mathbf{q}'$ , equation (A11) can be written as

$$\begin{aligned} \delta\mathbf{q}' &= \delta\mathbf{q} + [\mathbf{p} - \mathbf{p} + 2(\mathbf{n} \otimes \mathbf{n}) \mathbf{p}] \delta\tau_c \\ &= \delta\mathbf{q} + 2\delta\tau_c (\mathbf{n} \otimes \mathbf{n}) \mathbf{p}. \end{aligned} \quad (\text{A12})$$

For the momentum component  $\delta\mathbf{p}'$ , we get

$$\delta\mathbf{p}' = \mathbf{A} \delta\mathbf{q} + \mathbf{B} \delta\mathbf{p} + \delta\tau_c [\mathbf{p} \mathbf{A} + \omega \mathbb{S}] \quad (\text{A13})$$

$$\text{where } \mathbb{S} := \mathbf{B} \mathbf{R} - \mathbf{R} \mathbf{B} = 2 \begin{pmatrix} -2n_1 n_2 & n_1^2 - n_2^2 \\ n_1^2 - n_2^2 & 2n_1 n_2 \end{pmatrix}.$$

This can be simplified by using the fact that  $(\mathbf{b} \otimes \mathbf{a}) \mathbf{c} = \langle \mathbf{c}, \mathbf{a} \rangle \mathbf{b}$  and introducing the quantity  $\delta\mathbf{q}_c = \delta\mathbf{q} + \delta\tau_c \mathbf{p}$ , which represents the real space difference vector between the collision points of satellite and reference trajectories.

$$\begin{aligned} \delta\mathbf{p}' &= \delta\mathbf{p} - 2 \langle \delta\mathbf{p}, \mathbf{n} \rangle \mathbf{n} - 2 \frac{\partial \mathbf{n}}{\partial \mathbf{q}} (\langle \mathbf{p}, \delta\mathbf{q}_c \rangle \mathbf{n} + \\ &\quad \langle \mathbf{p}, \mathbf{n} \rangle \delta\mathbf{q}_c) + \delta\tau_c \omega \mathbb{S} \mathbf{p}. \end{aligned} \quad (\text{A14})$$

Using geometric considerations outlined by DPH we can now rewrite the penultimate term to get

$$\delta\mathbf{p}' = \delta\mathbf{p} - 2 \langle \delta\mathbf{p}, \mathbf{n} \rangle \mathbf{n} - 2\gamma_R \frac{\langle \delta\mathbf{q}, \mathbf{e} \rangle}{\cos \phi} \mathbf{e}' + \delta\tau_c \omega \mathbb{S} \mathbf{p} \quad (\text{A15})$$

where  $\phi$  is the angle of incidence,  $\gamma_R$  is the local curvature of the obstacle and  $\mathbf{e}$  and  $\mathbf{e}'$  are unit vectors orthogonal to  $\mathbf{p}$  and  $\mathbf{p}'$  respectively.

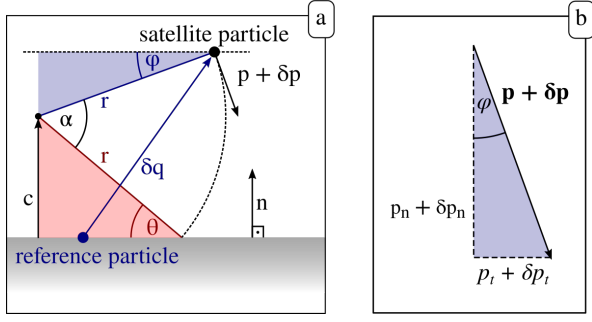


FIG. 7. (a) Geometric derivation of  $\delta\tau_c$ . As all spatial perturbations are small, it is sufficient to approximate the obstacle as a straight line. In this example, the satellite particle collides after the reference particle. (b) Decomposition of momentum into normal and tangential components

### 3. Collision delay time

The quantity  $\delta\tau_c$  in eqs. (A3) and (A11) can be interpreted as the time delay in between the collisions of the reference trajectory  $\Gamma$  and its satellite  $\Gamma + \delta\Gamma$ .

It can be computed by determining the signed distance from the satellite to its collision point measured along its trajectory at the time  $t_j(\Gamma)$  of the collision of the reference particle. As we are considering the linearized dynamics of the perturbation and Eq. (A3) is valid only to the first order of  $\delta\Gamma$ , we will ignore all higher orders of  $\delta\Gamma$  in the subsequent calculations.

Furthermore, we will denote vector components in normal direction of the obstacle by a subscript  $n$ , i.e.  $a_n = \langle \mathbf{a}, \mathbf{n} \rangle$ . Similarly, the tangential component of a vector will be denoted by a subscript  $t$ .

Geometrically, one can immediately derive the following two relations from the two triangles highlighted in Fig. 7a

$$\rho \sin \phi = \langle \delta \mathbf{q}, \mathbf{n} \rangle - \langle \mathbf{c}, \mathbf{n} \rangle \quad (\text{blue triangle}) \quad (\text{A16})$$

$$\rho \sin \theta = \langle \mathbf{c}, \mathbf{n} \rangle \quad (\text{red triangle}) \quad (\text{A17})$$

where  $\mathbf{c}$  is a vector between the obstacle and the cyclotron centre, as shown in fig. 7a. Eliminating the factor  $\langle \mathbf{c}, \mathbf{n} \rangle$  yields

$$\sin \theta = \frac{\langle \delta \mathbf{q}, \mathbf{n} \rangle}{\rho} - \sin \phi. \quad (\text{A18})$$

By construction,  $\theta$  cannot exceed  $\frac{\pi}{2}$  in absolute value. Therefore, we can safely apply the arcsine function to eq. (A18), receiving an expression for  $\theta$ .

$$\theta = \arcsin \left( \frac{\langle \delta \mathbf{q}, \mathbf{n} \rangle}{r} - \sin \phi \right). \quad (\text{A19})$$

We can now use this to compute the angle  $\alpha$  corresponding to the arc the particle has to travel during  $\delta\tau_c$ .

Using Fig. 7a, we can determine an expression for  $\alpha$

$$\alpha = \phi + \theta$$

$$\stackrel{\text{Eq. (A19)}}{=} \phi + \arcsin \left( \frac{\langle \delta \mathbf{q}, \mathbf{n} \rangle}{r} - \sin \phi \right). \quad (\text{A20})$$

This can be further simplified by expressing  $\phi$  in terms of the satellite particle's momentum (compare fig. 7b).

$$\alpha = \underbrace{\arcsin \left( \frac{p_t + \delta p_t}{\|\mathbf{p} + \delta \mathbf{p}\|} \right)}_K + \underbrace{\arcsin \left( \frac{\langle \delta \mathbf{q}, \mathbf{n} \rangle}{r} - \frac{p_t + \delta p_t}{\|\mathbf{p} + \delta \mathbf{p}\|} \right)}_L. \quad (\text{A21})$$

We can now linearize Eq. (A21) to receive our final result for  $\alpha$ . As the individual terms are somewhat complicated, but very similar, we will treat them separately. The first-order Taylor expansion of leftmost term is

$$K \approx \arcsin \left( \frac{p_t}{\|\mathbf{p}\|} \right) + \zeta(\delta \mathbf{p}_t) \quad (\text{A22})$$

where  $\zeta$  is of the form  $a \cdot \delta p_t + b \cdot \delta p_n$  with  $a, b$  given by the respective partial derivatives. Expanding the rightmost term in (A21) yields the similar result of

$$L \approx \arcsin \left( -\frac{p_t}{\|\mathbf{p}\|} \right) - \zeta(\delta \mathbf{p}_t) + \frac{1}{\sqrt{1 - p_t^2}} \cdot \frac{\langle \delta \mathbf{q}_i, \mathbf{n} \rangle}{r}. \quad (\text{A23})$$

This simplifies the final result for  $\alpha$  significantly. Using the anti-symmetry of the arcsine function, we can see that most of (A22) and (A23) cancel out, leaving only

$$\alpha = \frac{1}{\sqrt{1 - p_t^2}} \cdot \frac{\langle \delta \mathbf{q}, \mathbf{n} \rangle}{r}. \quad (\text{A24})$$

Finally, we have to multiply equation (A24) with the cyclotron radius  $r$ , then divide the resulting arclength by  $\|\mathbf{p}\|$  to get  $\delta\tau_c$

As  $\|\mathbf{p}\| = 1$  per convention, we can substitute  $\sqrt{1 - p_t^2} = |p_n|$ . However, we know that  $p_t < 0$  as the reference particle must have been moving towards the obstacle to collide with it. Therefore, we can further simplify our result to obtain

$$\delta\tau_c = -\frac{\langle \delta \mathbf{q}, \mathbf{n} \rangle}{\langle \mathbf{p}, \mathbf{n} \rangle}. \quad (\text{A25})$$

This is the same result as for linear propagation in [23, Eq. 18], since higher orders of  $\delta\Gamma$  were neglected.

Combining eqs. (A12), (A15) and (A25), we receive a final result for of

$$\delta\Gamma' = \left( \begin{array}{c} \delta \mathbf{q} - 2(\delta \mathbf{q} \cdot \mathbf{n}) \mathbf{n} \\ \delta \mathbf{p} - 2(\delta \mathbf{p} \cdot \mathbf{n}) \mathbf{n} - 2\gamma_r \frac{\langle \delta \mathbf{q}, \mathbf{e} \rangle}{\cos \phi} \mathbf{e}' \end{array} \right) - \omega \frac{(\delta \mathbf{q} \cdot \mathbf{n})}{(\mathbf{p} \cdot \mathbf{n})} \left( \begin{array}{c} 0 \\ \mathbb{S} \cdot \mathbf{p} \end{array} \right). \quad (\text{A26})$$

## Appendix B: Mean return time to stem

In this section, we will derive an analytic expression for the mean return time to the stem bottom in a mushroom billiard. Using Kac's lemma [33–35], which states that for volume-preserving maps, the mean number of iterations  $n_S$  required to return to a compact subset  $S$  of phase space is given by

$$n_S = \frac{\mu(A)}{\mu(S)} \quad (\text{B1})$$

where  $\mu(\cdot)$  is the volume of a set and  $A$  is the subset of phase space accessible to orbits originating in  $S$ .

To transform the billiard flow into a map, we discretize time in small steps  $\Delta t$ , implicitly considering the limit of  $\Delta t \rightarrow 0$ . We now choose the set  $S$  of momenta and positions defined by

$$S = \{\mathbf{q} \in Y, p_y > 0\} \quad (\text{B2})$$

where  $Y$  is a box of width  $w$  and height  $\epsilon$  at the bottom of the stem. The phase space volume of  $S$  is  $\mu(S) = \pi w \epsilon$  in the limit of  $\Delta t \rightarrow 0$ . As the chaotic phase space section of mushroom billiards is ergodic [30], we know that the measure of the subset  $A$  of phase space accessible from  $S$  is given by the volume of chaotic phase space  $V_{\text{CH}} = V_{\text{TOT}} - V_{\text{REG}}$ .

Applying Kac's lemma to get the mean iterations to return to the stem and multiplying by  $\Delta t$ , we get a result for the mean return time  $\kappa_S(h, w, r)$  to the set  $S$ .

$$\kappa_S(h, w) = \frac{V_{\text{CH}}(h, w)}{\pi \epsilon w} \Delta t. \quad (\text{B3})$$

To eliminate  $\Delta t$ , we divide by  $\kappa_S$  for  $w = 2$  to get

$$\kappa_S(h, w) = \frac{V_{\text{CH}}(h, w)}{V_{\text{TOT}}(h, 2)} \frac{2}{w} \kappa_S(h, 2). \quad (\text{B4})$$

As this equation no longer depends on  $\epsilon$ , we can now take the limit  $\epsilon \rightarrow 0$ .

We can find  $\kappa_S(h, 2)$  because of the ergodicity of the MB for  $w = 2$ . Specifically, it holds that  $\kappa_S(h, 2) = n_S(h) \times \tau$  with  $n_S$  the mean amount of iterations to return to the stem and  $\tau$  the mean collision time in the MB given by Eq. (3). We consider the boundary map of the billiard (Birkhoff coordinates),  $(\xi, \sin \phi_n)$ , with  $\xi$  the coordinate along the boundary (i.e. the arc-length) and  $\phi_n$  the angle of incidence with respect to the normal vector at  $\xi$ . This coordinate system is a discrete mapping and Kac's lemma applies directly. Therefore the mean iterations to return to the stem bottom are

$$n_S = \frac{2|\partial Q|}{2 \cdot 2} \quad (\text{B5})$$

where  $|\partial Q|$  is the perimeter the boundary (the explicit factor of 2 represents the contribution of  $\sin \phi_n$ ). Using Eq. (3), we find

$$\tau = \frac{\pi \cdot (2h + \pi/2)}{|\partial Q|}. \quad (\text{B6})$$

Combining eqs. (B5) and (B6), we receive an expression for the mean stem return time in the fully ergodic case

$$\kappa_S(h, 2) = \frac{\pi}{2} (2h + \pi/2). \quad (\text{B7})$$

## Appendix C: Mean duration of chaotic episodes

A chaotic episode in the MB as defined above consists of the particle travelling from the cap head directly into to the stem and back up to the cap head, without any other collisions inside the cap. To determine the mean duration  $\tau_c$  of these episodes, we can geometrically determine the average lengths of the trajectories, exploiting that all trajectories are uniquely defined by the angle of incidence  $\alpha$  and the distance  $\delta$  from the cap center at which they enter the stem.

To simplify the calculation, it is useful to split the trajectory into the mean length of cap transit  $\langle c \rangle$  and the mean length of stem transit  $\langle s \rangle$  where  $\tau_c = 2 \langle c \rangle + 2 \langle s \rangle$ .

The stem transit length can be easily computed using simple trigonometry and depends only on the angle  $\alpha$

$$s = \frac{h}{\cos(\alpha)}. \quad (\text{C1})$$

As the directions of particle momenta are equidistributed, we know that  $\alpha$  must be cosine-distributed. We can now integrate over  $\alpha$  to obtain the mean  $s$ , finding

$$\langle s \rangle = \int \frac{h}{\cos \alpha} \frac{1}{2} \cos(\alpha) d\alpha = \pi h. \quad (\text{C2})$$

Determining the cap transit length is more difficult as it depends both on  $\alpha$  and  $\delta$ . Using the law of sines, we can derive

$$c = \frac{r}{\cos(\alpha)} \cos \left( \arcsin \left( \frac{\delta}{r} \cos \alpha \right) - \alpha \right). \quad (\text{C3})$$

To get an average result, this expression has to be integrated both over  $\delta$  and  $\alpha$ , again using the fact that  $\alpha$  is cosine-distributed. Unfortunately, we were unable to solve the integrals analytically. Therefore, we decided to approximate  $\int c d\delta$  by a polynomial before performing the second integration, yielding

$$\langle c \rangle \approx 1 - \frac{w^2}{36} - \frac{w^4}{1200} - \dots \quad (\text{C4})$$

- 
- [1] Y. G. Sinai, *Russ. Math. Surv.* **25**, 137 (1970).
- [2] L. A. Bunimovich, *Funct Anal Its Appl* **8**, 254 (1974).
- [3] L. A. Bunimovich, *Commun.Math. Phys.* **65**, 295 (1979).
- [4] H.-J. Stöckmann and J. Stein, *Phys. Rev. Lett.* **64**, 2215 (1990).
- [5] A. H. Barnett and T. Betcke, *Chaos Interdiscip. J. Nonlinear Sci.* **17**, 043125 (2007).
- [6] A. D. Stone, *Nature* **465**, 696 (2010).
- [7] C. Gmachl, F. Capasso, E. E. Narimanov, J. U. Nöckel, A. D. Stone, J. Faist, D. L. Sivco, and A. Y. Cho, *Science* **280**, 1556 (1998).
- [8] S. Koyanagi, T. Nakano, and T. Kawabe, *J. Acoust. Soc. Am.* **124**, 719 (2008).
- [9] G. Datsleris, T. Geisel, and R. Fleischmann, arXiv:1711.05833 [cond-mat, physics:nlin] (2017), arXiv:1711.05833 [cond-mat, physics:nlin].
- [10] R. Fleischmann, T. Geisel, and R. Ketzmerick, *Physical Review Letters* **68**, 1367 (1992).
- [11] D. Weiss, M. L. Roukes, A. Menschig, P. Grambow, K. von Klitzing, and G. Weimann, *Phys. Rev. Lett.* **66**, 2790 (1991).
- [12] N. I. Chernov, G. L. Eyink, J. L. Lebowitz, and Y. G. Sinai, *Commun.Math. Phys.* **154**, 569 (1993).
- [13] R. Yagi, R. Sakakibara, R. Ebisuoka, J. Onishi, K. Watanabe, T. Taniguchi, and Y. Iye, *Physical Review B* **92**, 195406 (2015).
- [14] H. Maier, J. Ziegler, R. Fischer, D. Kozlov, Z. D. Kvon, N. Mikhailov, S. A. Dvoretzky, and D. Weiss, *Nature Communications* **8**, 1 (2017), arXiv:1708.07766.
- [15] S. Chen, Z. Han, M. M. Elahi, K. M. M. Habib, L. Wang, B. Wen, Y. Gao, T. Taniguchi, K. Watanabe, J. Hone, A. W. Ghosh, and C. R. Dean, *Science* **353** (2016), 10.1126/science.aaf5481, arXiv:1602.08182.
- [16] J. P. Bird, ed., *Electron Transport in Quantum Dots* (Springer US, 2003).
- [17] C. Beenakker, in *Quantum Dots: a Doorway to Nanoscale Physics* (Springer Berlin Heidelberg, 2005) pp. 131–174.
- [18] L. A. Ponomarenko, F. Schedin, M. I. Katsnelson, R. Yang, E. W. Hill, K. S. Novoselov, and A. K. Geim, *Science* **320**, 356 (2008).
- [19] N. Chernov, *J. Stat. Phys.* **88**, 1 (1997).
- [20] N. Chernov and L. S. Young, in *Hard Ball Systems and the Lorentz Gas*, Encyclopaedia of Mathematical Sciences (Springer, Berlin, Heidelberg, 2000) pp. 89–120.
- [21] N. Chernov and R. Markarian, *Chaotic Billiards*, mathematic ed. (American Mathematical Society, 2006) p. 328.
- [22] C. Dellago and H. A. Posch, *Phys. Rev. E* **52**, 2401 (1995).
- [23] C. Dellago, H. A. Posch, and W. G. Hoover, *Phys. Rev. E* **53**, 1485 (1996).
- [24] P. Gaspard and F. Baras, *Phys. Rev. E* **51**, 5332 (1995).
- [25] H. A. Posch and R. Hirschl, in *Hard Ball Systems and the Lorentz Gas*, Encyclopaedia of Mathematical Sciences (Springer, Berlin, Heidelberg, 2000) pp. 279–314.
- [26] O. Meplan, F. Brut, and C. Gignoux, *J. Phys. Math. Gen.* **26**, 237 (1993).
- [27] Z. Vörös, T. Tasnádi, J. Cserti, and P. Pollner, *Phys. Rev. E* **67** (2003), 10.1103/PhysRevE.67.065202.
- [28] L. A. Bunimovich, *Nonlinearity* **31**, R78 (2018).
- [29] G. Datsleris, *J. Open Source Softw.* **2**, 458 (2017).
- [30] L. A. Bunimovich, *Chaos Interdiscip. J. Nonlinear Sci.* **11**, 802 (2001).
- [31] E. G. Altmann, A. E. Motter, and H. Kantz, *Chaos* **15** (2005), 10.1063/1.1979211.
- [32] E. G. Altmann, A. E. Motter, and H. Kantz, *Physical Review E - Statistical, Nonlinear, and Soft Matter Physics* **73**, 1 (2006).
- [33] M. Kac, *Bull. Amer. Math. Soc.* **53**, 1002 (1947).
- [34] R. S. MacKay, *J Nonlinear Sci* **4**, 329 (1994).
- [35] J. D. Meiss, *Chaos* **7**, 139 (1997).